EVALUATING THE IN-PLANE BEHAVIOUR OF 3D PRINTED CONCRETE SHEAR WALLS UNDER QUASI STATIC REVERSED CYCLIC LOADING

Hentschel[1], Alexander, Fam[2], Amir, and Woods[3], Joshua

[1]Graduate Student, Department of Civil Engineering, Queen's University, Ellis Hall, Kingston, ON K7L 3N6, Canada. E-mail: alexander.hentschel@queensu.ca
[2]Canada Research Chair and Vice Dean (Research), Department of Civil Engineering, Queen's University, Ellis Hall, Kingston, ON K7L 3N6, Canada. E-mail: amir.fam@queensu.ca
[3]Assistant Professor, Department of Civil Engineering, Queen's University, Ellis Hall, Kingston, ON K7L 3N6, Canada. E-mail: joshua.woods@queensu.ca (Corresponding Author)

ABSTRACT

Additive manufacturing of low-rise residential and commercial buildings using printed cementitious materials, a technology that is commonly referred to as 3D concrete printing (3DCP), is now being deployed at scale across North America. A significant challenge in expanding the use of 3DCP is the incorporation of longitudinal steel reinforcement and understanding their structural performance under earthquake loads. This study examines the performance of longitudinal steel reinforcement in the cavities of 3D printed concrete shear walls evaluates their structural behaviour under in-plane reversed cyclic loading. The work also investigates the influence of boundary element reinforcement detailing, shear wall aspect ratio (ratio of the wall height to its length), and the type of horizontal shear reinforcement (steel versus glass fiber-reinforced polymer (GFRP) bars), and axial load on wythe behaviour. Digital image correlation (DIC) is used to capture full-field displacement and strain distributions in the walls as well as crack widths. Results show that 3DPC shear walls exhibit cyclic behaviour that is different when compared to conventional reinforced concrete design. The response of the walls was found to be highly dependent on the strength of the base connection, and in cases when the base connection was under-designed, the wall behaved more like a precast or rocking wall system under in-plane loads. The use of horizontal shear reinforcement between layers of 3DPC was found to be effective at improving the diagonal tension capacity of the walls.

Keywords: 3D concrete printing, additive manufacturing, shear walls, earthquake loading, longitudinal, reinforcement, in-plane loading, digital image correlation

INTRODUCTION

The global construction industry is increasingly challenged by skilled labour shortages and the need to improve productivity, driving interest in innovative construction methods. Compared with sectors such as manufacturing, construction has traditionally been slower to adopt technological advancements due to the complexity of site conditions and the unique nature of individual projects [1]. Nevertheless, recent years have seen growing attention toward technologies capable of enhancing construction efficiency through automation and robotics. One such technology is three-dimensional concrete printing (3DCP), an additive manufacturing process in which a robotic arm or gantry system deposits layers of fresh concrete to create structural components. By eliminating the need for conventional formwork and reducing reliance on skilled labour, 3DCP offers the potential to increase construction efficiency while minimizing material waste relative to traditional construction practices [2,3].

Despite its promise, 3DCP remains an emerging technology, and significant uncertainties persist regarding its structural performance [3]. Existing knowledge has been comprehensively reviewed in several recent state-of-the-art studies [4–6]. To date, research has largely concentrated on material-level behaviour, including printability requirements, rheological properties, mixture composition, compressive and tensile strength, and interlayer bond performance [4–6].

In contrast, comparatively limited attention has been devoted to the structural response of 3DCP components and assemblies, such as walls and columns. Experimental investigations have examined wall performance under concentric axial compression [7–9], eccentric compression [10], and in-plane cyclic lateral loading [11–13]. A recurring challenge across these studies is the incorporation of longitudinal reinforcement. For multi-storey structures or buildings located in regions of elevated seismic hazard, longitudinal reinforcement is essential to satisfy strength requirements and ensure adequate ductility during earthquake events. Extensive evidence demonstrating the poor seismic performance of unreinforced masonry under both in-plane [14,15] and out-of-plane loading [16] suggests that similar vulnerabilities may exist in unreinforced 3DCP structures.

Although the necessity of longitudinal reinforcement in 3DCP elements is widely acknowledged, there remains no consensus regarding an efficient and practical implementation strategy [17,18]. In conventional reinforced concrete construction, vertical reinforcement is installed prior to concrete placement. However, this approach is incompatible with the layer-by-layer printing process, as the reinforcement would obstruct the movement of the printing nozzle. While recent reviews have demonstrated that reinforcement oriented parallel to the printing plane can be successfully integrated between layers without adversely affecting bond or pull-out performance [19–21], equivalent solutions for reinforcement perpendicular to the printed layers remain limited.

Several methods have been proposed to address this challenge, including the incorporation of reinforcement within cavities formed during printing, followed by grouting either during or after the printing process [11]. This approach is analogous to reinforced masonry construction and has proven effective; however, it diminishes some of the productivity advantages associated with 3DCP due to the additional labour and time required for reinforcement placement and grouting. Nonetheless, it is considered one of the most practical and readily implementable reinforcement strategies for near-term industry adoption and was therefore selected for the present study. Despite its potential, considerable uncertainty remains regarding the seismic behaviour of reinforced 3DCP walls. Fewer than five experimental studies have reported on the in-plane response of 3DCP shear walls under earthquake-type loading, highlighting the need for additional experimental evidence. In particular, further research is required to evaluate the influence of reinforcement detailing and the layered construction process on the seismic performance of 3DCP wall systems.

This study aims to address some of these knowledge gaps and evaluates the seismic behaviour of eight full-scale 3DPC shear walls with varying design details under in-plane reversed cyclic loading. The specific objective of this research is to: (1) examine the in-plane stiffness, strength, ductility, and energy dissipation capacity of 3DPC shear walls under in-plane loading, (2) study the influence of axial load ratio, boundary element reinforcement detailing, and the presence of horizontal shear reinforcement (both steel and GFRP bars) on strength and ductility, and (3) Use digital image correlation to study the displacement, strain (and stress) distributions in full-scale 3DCP wall panels.

EXPERIMENTAL PROGRAM

The experimental program consisted of 8 full-scale 3DPC shear wall panels with varying reinforcement details. The specimens included those with varying boundary element detailing (e.g., with and without confinement), and reinforcement configuration, including the presence of diagonal reinforcement as well as horizontal steel shear or GFRP reinforcement.

Wall Panel Specimens

Figure 1 shows the geometry of the shear wall specimens. The walls panels measured 2650 mm tall and 300 mm thick, which consisted of two exterior wythe veneers and an interior zig-zag pattern. The length of the wall was either 1350 mm or 1950 mm, which resulted in height-to-length aspect ratios of approximately 2.0 and 1.35, respectively. These aspect ratios were selected to investigate two different types of shear wall behaviour: (1) slender wall behaviour in walls with aspect ratios of 2.0 or more, the response of which is governed predominantly by flexural deformations, and (2) intermediate wall behaviour in walls with aspect ratios between 1.0 and 2.0, in which the response of the wall is expected to be governed by a both shear and flexural deformations. Each wall specimen included a heavily reinforced foundation block and cap beam, which measured 350 mm and 320 mm tall, respectively, and were designed to remain uncracked during testing of the walls. This specimen geometry resulted in a flexural lever arm of approximately 2815 mm to the centre of the cap beam, which would be representative of a wall in a single storey home or the first-storey wall of a multi-storey structure. One of the unique aspects of the shear wall design relative to conventional reinforced concrete or masonry construction was the configuration of the longitudinal reinforcement and the presence of lap splices along the wall height, which are shown in Figure 1. These were necessary to accommodate the space requirements of the printer and the construction sequence to accomplish this design is discussed in a subsequent section of this paper.

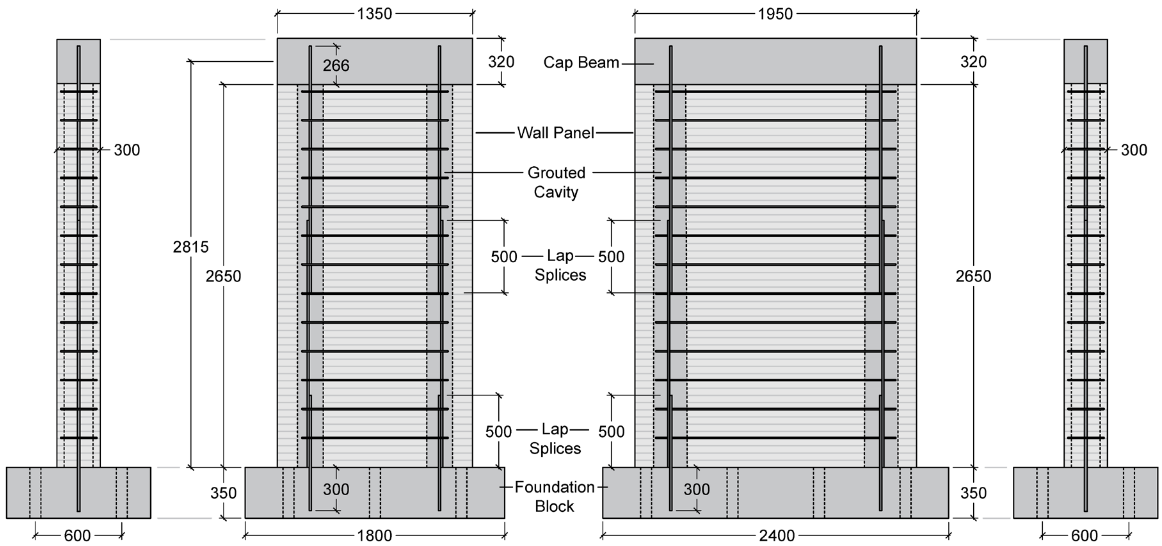

Figure 1. Specimen geometry: (a) 2.0 aspect ratio walls, (b) 1.35 aspect ratio walls.

Figure 2 shows the cross-sections of the shear walls tested in this study. Different boundary element details and horizontal shear reinforcement types were considered, which are summarized in Table 1. For the 2.0 aspect ratio walls, referred to as the 'slender walls' and denoted walls S1-S4 in Table 1, the area of the longitudinal reinforcement in the boundary element remained constant, which included either 1-20M (d_b = 19.5 mm, $A_b = A_r$ = 300 mm^2) in Wall S-1, S-2, and S-3 or 3-10M (d_b = 11.3 mm, A_b = 100 mm^2, A_r = 300 mm^2) in wall S-4. The walls with a single longitudinal reinforcing bar at each end were intended to represent conventional construction practices that an engineer might use in low-seismic zones, where confinement and design for higher ductility may not be required. In contrast, the wall with three longitudinal reinforcing bars in a tied column were intended to be achieve a higher level of seismic performance. Because the wall cavity was small, fabricating closed ties for the vertical reinforcement was a challenge. Instead, a spiral wire (9 gauge with db = ~3.76 mm) was used with a spiral spacing of approximately 50 mm. The final design parameter varied amongst the slender walls (2.0 aspect ratio) was the presence and type of horizontal shear reinforcement. One was tested without shear reinforcement and potentially force a diagonal tension shear failure. The other slender walls had either steel or GFRP shear reinforcement spaced at 200 mm on centre, which was determined to be sufficient to carry the shear associated with the predicted flexural strength of the walls.

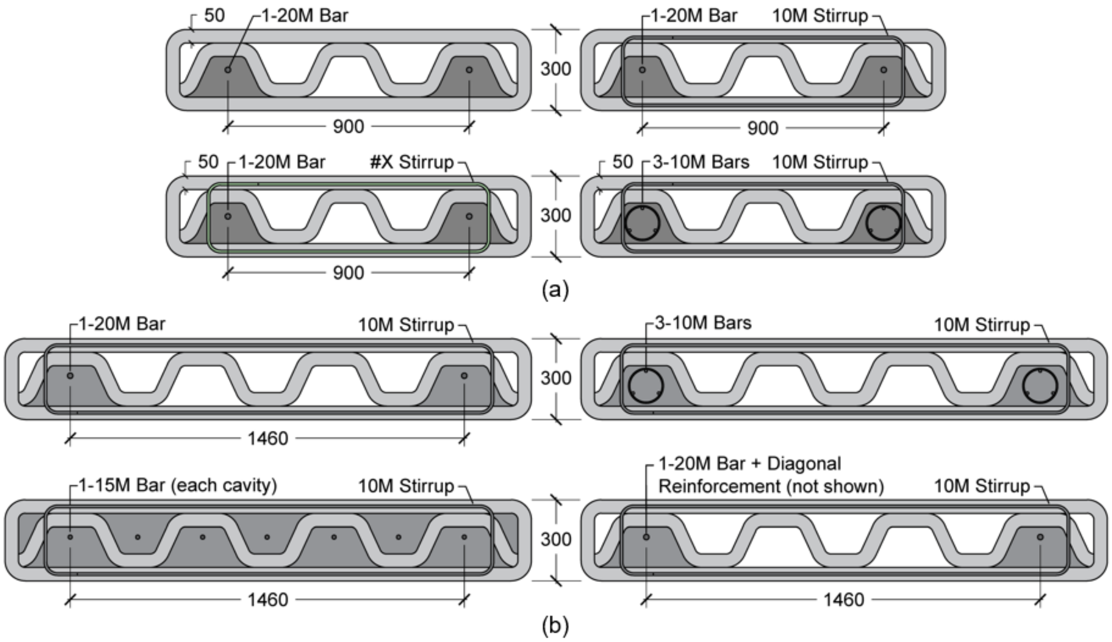

Figure 2. Shear wall cross-section details: (a) slender walls with aspect ratio of 2.0, including walls with and without shear reinforcement and different boundary element details, (b) intermediate walls with aspect ratio of 1.35, including walls with different boundary element details (see Table 1).

Table 1. Test matrix and specimen geometry

Name	**Dimension ($l_w \times t_w$) (mm)**	**Aspect Ratio (h_w/l_w)**	**Vertical Steel Reinforcement**	**Horizontal steel Reinforcement**
S1	1350	2.0	1-20M	-
S2	1350	2.0	1-20M	10M@200
S3	1350	2.0	1-20M	#4@200
S4	1350	2.0	3-10M	10M@200
I1	1950	1.35	1-20M	10M@200
I2	1950	1.35	3-10M	10M@200
I3	1950	1.35	7-15M	10M@200
I4	1950	1.35	2-10M+Diagonal*	10M@200

* Reinforcement consisted of 2 diagonally oriented 20M bars in a grouted cavity

The four full-scale intermediate walls (aspect ratio of 1.35) had several similar design details to the slender walls. All walls had either steel horizontal shear reinforcement. As shown in Figure 2, two had with similar longitudinal reinforcement areas, including one wall (Wall I1) with 1-20M bar (d_b = 19.5 mm, A_b =

A_r = 300 mm^2) and confined column boundary elements (Wall I2) with 3-10M (d_b = 11.3 mm, A_b = 100 mm^2, A_r = 300 mm^2) in a tied column. The two new design details tested in the intermediate walls included a wall with distributed reinforcement (Wall I3), which had 1-15M bar (d_b = 15.9 mm, A_b = 200 mm^2, A_r = 1400 mm^2). This design detail was intended to be representative of a section of a longer shear wall along a building length, where the designing may choose to reinforce and grout each cell. The last shear wall in the series (Wall I4), had a unique cross-section detail that attempted to maximize the benefits of 3DCP. In this wall, four cavities were printed, including two at the wall ends and two diagonal cavities, as shown in Figure 3. The diagonal cavities are formed by varying the wall cross-section at each layer. To reinforce the wall, 1-20M bar (d_b = 19.5 mm, A_b = A_r = 300 mm^2) was placed in each cell.

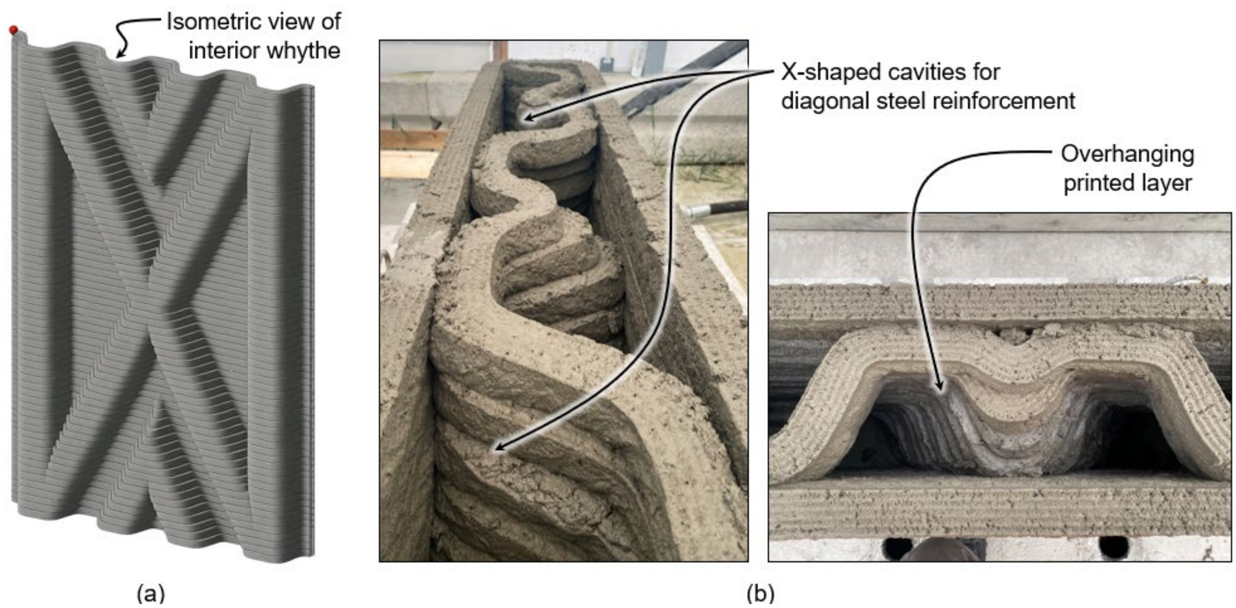

Figure 3. Design details for diagonally reinforced shear wall:

Shear Wall Fabrication

To fabricate the full-scale walls, a three-axis gantry-type extrusion system (COBOD BOD2) was used. The printer speed varied between approximately 100 mm/s and 180 mm/s, which resulted in a layer time of approximately 10-15 minutes, which was selected to represent a layer time that might be used in practice. It is noted that a slightly slower print speed and layer time was required in the diagonally reinforced wall (Wall I4), because of the need for the overhanding layer to harden more compared to the other walls in which a fresh layer was always fully supported by an underlying layer.

The walls were printed in several phases to accommodate placement of the vertical reinforcement, as summarized in Figure 4. First, the reinforced concrete foundation block was cast followed by printing of the first 4 layers of each wall. At this point, the first stirrup was placed, which continued every 4 layers throughout the entire construction sequence. As previously noted, because of the space requirements of the printer during printing, the longitudinal reinforcement could not be continuous. Consequently, a lap splice was used at the base of the wall, as typical detail for this is shown in Figure 4. In this configuration, the first 10 layers (roughly 500 mm of wall height) was printed first, and then a ~1000 mm long segment of bar was bonded into the wall foundation using an epoxy adhesive. The total design embedment length was 300 mm into the foundation block and a 500 mm long lap splice. After installation of the bar, the next 24 layers of the wall were printed (1700 mm of total wall height). At this point, a second bar was placed in the cavity, again with a target lap splice length of 500 mm and the cavity was filled with a grout material. Finally, the wall was printed up to its final height of 53 layers (2650 mm of total wall height) after which the final reinforcing bar segment was placed and the cavity was grouted to the top of the wall. After completing the printed layers, a reinforced concrete cap beam was added to the top of the wall specimen, in which the longitudinal reinforcement was embedded approximately 265 mm.

This procedure was used for all wall specimens, irrespective of specific boundary element detail, and select photos of the wall specimens during the printing process are shown in Figure 5. It is noted that the need to top to place vertical reinforcement and grout the cavities for structural stability of the wall does result in a cold joint at several locations along the wall height (including at 500 mm and 1700 mm), the structural implications of which are discussed in subsequent sections of this paper. This same construction sequencing would likely be required on site during construction of a house or multi-storey structure, and so, it is a realistic scenario that could occur in the field for the same reason or between work shifts.

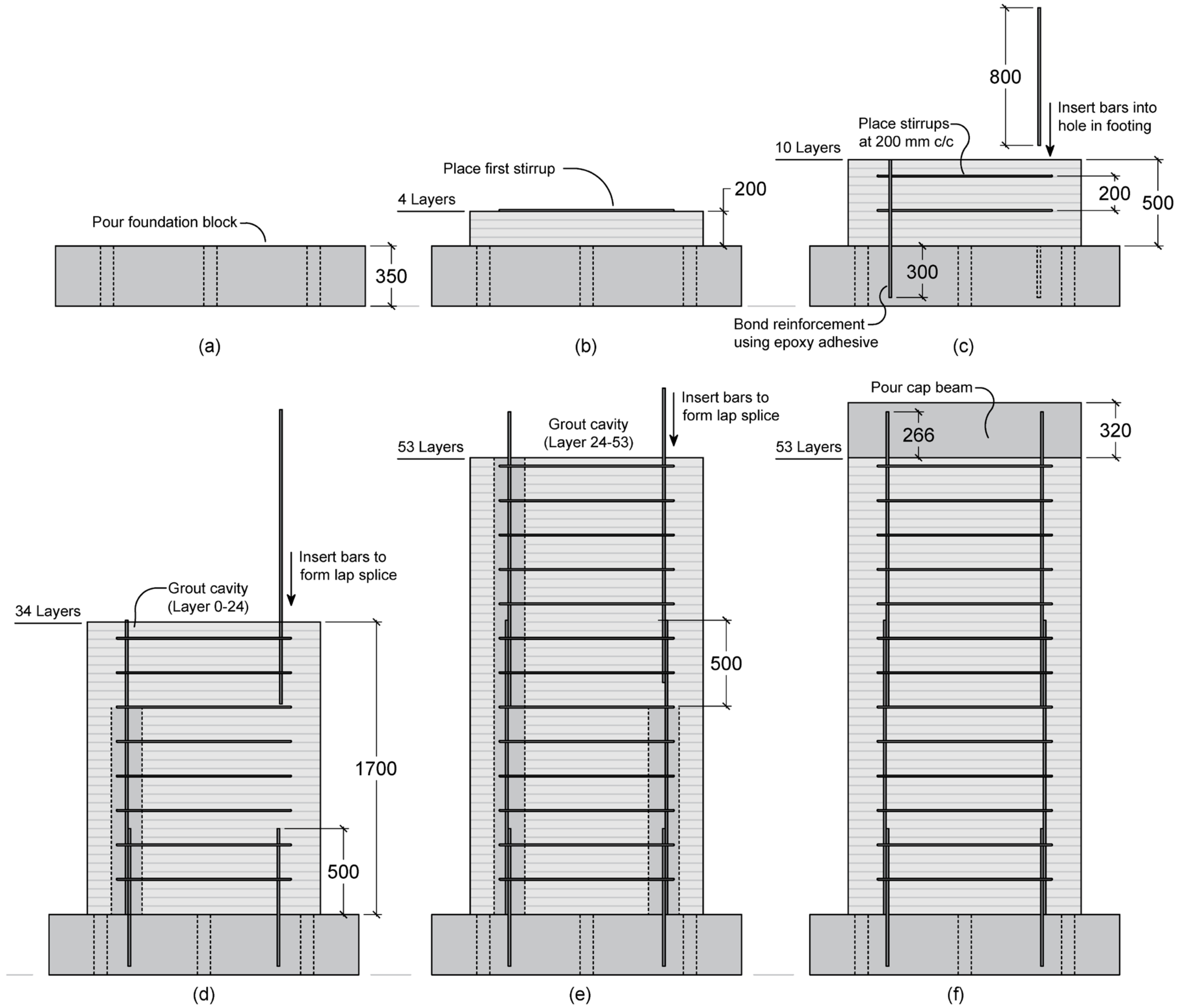

Figure 4. Shear wall fabrication sequence: (a) cast foundation block, (b) print first four layers and place first stirrup (subsequently spaced at 200 mm on centre), (c) drill holes in foundation and place embed vertical reinforcing bars, (d) print up to layer 34 and place subsequent reinforcing bar, (e) print up to layer 53 and place final reinforcing bar, (f) place reinforcement and pour concrete cap beam.

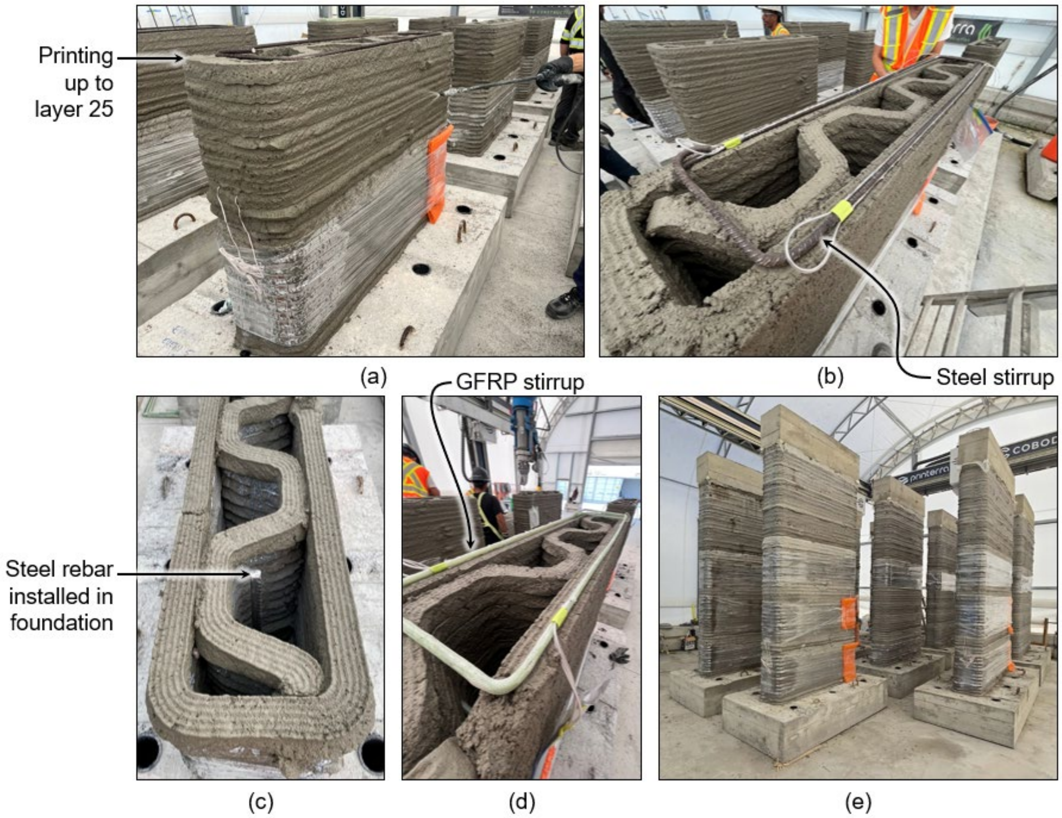

Figure 5. Shear wall fabrication sequence: (a) completion of printing up to approximately layer 30, (b) typical placement of a steel stirrup (subsequently spaced at 200 mm on centre), (c) typical installation of the vertical steel reinforcing bar, (d) typical placement of a GFRP stirrup, (e) completed shear wall specimens after printing and casting reinforced concrete cap beam.

Material Properties

3D Printed Concrete: material properties of the 3DCP in this study were assessed using specimens that were saw-cut from the printed shear wall. The 3DCP mix included GUL cement (650 kg/m^3), fine aggregate (1100 kg/m^3), 5 mm coarse aggregate (420 kg/m^3), and water (120 L/m^3). Additives to the concrete mixture included superplasticizer, air entrainment (0.6L/m^3), and monofilament microsynthetic fiber (0.6kg/m^3) to reduce plastic shrinkage cracking. The mortar used to fill the printed cavities has the same properties as the printed concrete, with the exception of additional superplasticizer, which was used to improve flowability. The only other unique requirement during printing was for wall I4, which had the 'X-shaped' cavity. The cross-section geometry required that a portion of the printed layer overhand relative to the previous layer, as shown in Figure 3, to provide additional stability for the printed layer, additional stiffener was required at the tip of the printer to increase the curing time.

To the compression strength of the tests were carried out on prisms, which were saw-cut from the wall samples. The prisms were nominally 50 mm × 50 mm and were 155 mm tall, representing approximately three layers of printed material. The average compressive strength of the 3DCP prisms was 44.1 MPa (SD = 6.61 MPa). The modulus of rupture of the material was also evaluated through tests on prisms that were saw-cut from a 3DCP element. The modulus of rupture specimens followed the guidelines outlined in ASTM C78/C78M [31] and the printed concrete prisms had nominal dimensions of 50×50×240 mm. The modulus of rupture of the printed concrete prisms was 5.97 MPa (SD = 0.52 MPa).

Steel Reinforcement: the steel reinforcement was grade 400W and included bar sizes of 10M, 15M, and 20M with A_b = 100, A_b = 200, and A_b = 300 mm^2, respectively. Tensile tests on steel bars taken from the test samples were conducted according to the procedures outlined in ASTM E8/E8M [36]. Based on the results of the coupon tests, the steel reinforcement had average yield stresses (f_y) of 450 MPa.

GFRP Reinforcement: The horizontal shear reinforcement in select walls (see Table 1) was #4 GFRP reinforcement (MST-Bar Grade III) was a ribbed bar with A_b = 125 mm^2 cross-sectional area and had a reported elastic modulus of 60 GPa, a minimum tensile strength of 1000 MPa, and an ultimate strain of 1.7 % [35].

Test Setup and Instrumentation

The 3DCP shear walls were tested under a combination of axial load and in-of-plane loading, and Figure 6 shows a typical experimental test setup. The shear wall was fixed to the laboratory strong floor at its base and three servo-controlled hydraulic actuators were used to apply the load. Two vertically oriented actuators (+/- 250 kN, +/- 150 mm) were used to apply the gravity load. The vertical load was applied through a 310×158 steel spreader beam located in the centre of the top of the wall. The lateral displacement was applied using a horizontally-oriented actuator (+/- 500 kN, +/- 250 mm), which was connected to a steal reaction frame at one end and fixed around the wall cap beam using four 1” grade B7 threaded rods at the other. The actuator had hinges at both ends, ensuring no moments were produced at the top of the wall and that it behaved as a cantilever wall. A lateral restraint system prevented out-of-plane displacements at the top of the specimen, as shown in Figure 6.

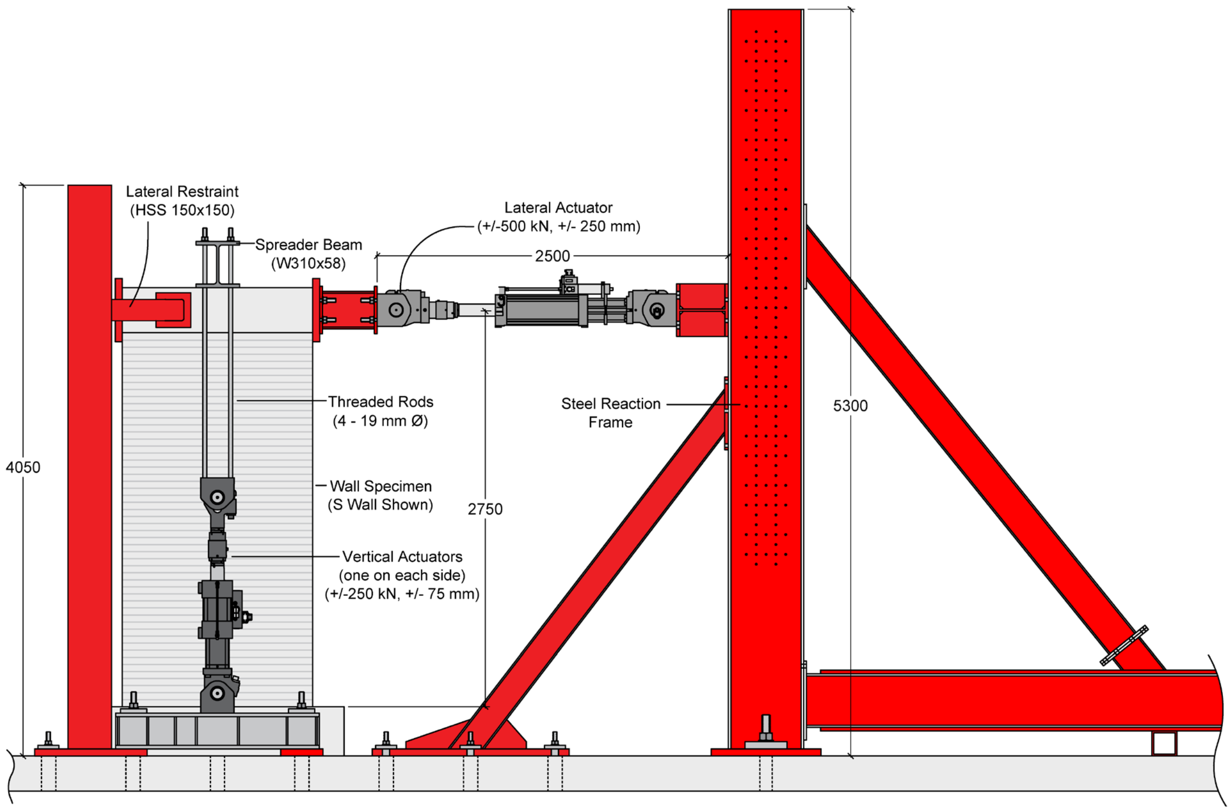

Figure 6. Illustration of multi-actuator experimental test setup and discrete instrumentation.

To measure the response of the wall during the test, both discrete and distributed sensors were employed. The loads were measured using load cells connected to the hydraulic actuators. Several discrete displacement transducers were used, including to measure the lateral displacement at the mid-height and top of the wall, sliding displacements at the base, and uplift at the base, and any sliding of the foundation block.

In addition to discrete sensors, strain distributions and displacement fields were also measured using distributed fiber optic strain sensors and digital image correlation. Digital image correlation was used to measure shear and flexural displacements over the surface of the wall as well as to monitor crack evolution. Figure 7 shows a photo of a typical test setup in the lab as well as the wall surface used for DIC analysis. Photos were taken throughout each test using two stereo cameras (5MP 2488x2048 with F1.4/17mm lenses) oriented vertical to enable the region of interest to span the entire wall surface. The surface of the wall was painted with a white basecoat and speckle pattern, which is also shown in Figure 7(b), where the speckle size (approximately 5 mm in diameter) was selected based on the position of the cameras relative to the region of interest and the size of the region of interest. DIC is particularly well-suited for this application because the surface of the concrete is so irregular, meaning installation of sensors and marking of cracks is a challenge. Furthermore, assessing whether cracks form along the layer-layer interfaces can also be difficult. In this study, the VIC-3D software was used for data analysis combined with the VIC-Snap software for data acquisition (Correlated Solutions, 2026). The rate of image capture during the test was 3-5 images/second.

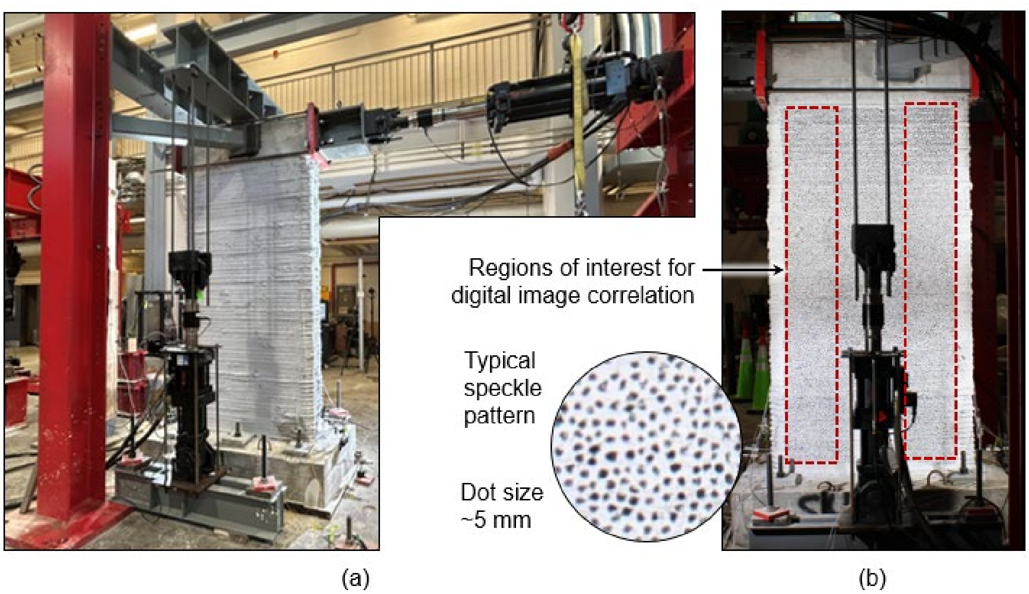

Figure 7. (a) typical experimental test setup in the laboratory, (c) digital image correlation configuration.

To measure distributed strain along the steel reinforcement in the 3DPC walls, select reinforcing bars were instrumented with distributed fibre optic strain sensors. Distributed fibre optic sensors use a laser with an optical fiber and measures changes in the reflected wavelength over the length of a fibre optic cable to infer mechanical/thermal strain. Additional background on the technology can be found in Hoult et al. (2010). In this study, Rayleigh backscattered-based fibre optic sensing technology was used, which combines high-resolution strain measurement (1–3 microstrain) with small sensor spacing (0.5-5 millimeters) and long fibre lengths (10-50 m). An ODiSI 6104 analyzer was used and data was sampled at 1 Hz throughout the test.

Figure 8 shows the configuration of the optical fiber on a typical longitudinal reinforcing bar as well as a stirrup. In both cases, nylon coated fibre optic cables (outer diameter 900 µm with core diameter of 250 µm) were used, which were adhered along the longitudinal ribs of the reinforcing bar. Both sides of the bar were instrumented to capture bar bending. Steps to installing the sensors included first sanding the longitudinal rib smooth, cleaning the rib with alcohol, and finally adhering the optical fiber using a cyanoacrylate adhesive. Finally, a thin layer of silicone was used to cover the fiber and provide protection during wall fabrication. Additional information on the use of fiber optic strain sensors in civil engineering applications as well as details on the background technology can be found in Hoult et al. [42].

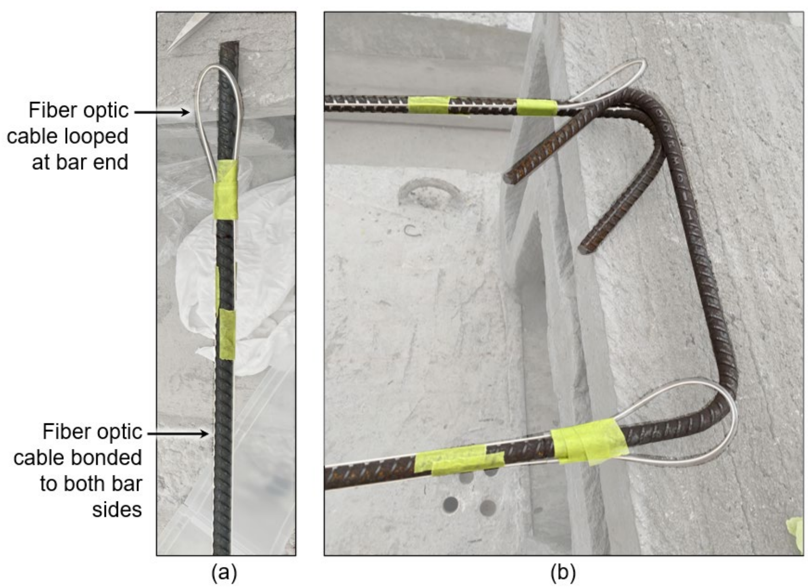

Figure 8. Typical installation of optic fibers on: (a) the longitudinal steel reinforcement and (b) the horizontal steel reinforcement.

Loading Protocol

To simulate the drift damage and damage to a 3DCP shear wall during a design-level earthquake, the walls were tested under quasi-static reversed cyclic loading up to failure. Figure 9 shows the cyclic loading protocol, which involved the application of both vertical (gravity) loading and in-plane cyclic loading. The vertical load was applied first over a period of 2 minutes. The total vertical load applied during the tests was 380 kN. It is noted that the resulting axial load ratio is small compared to what might be considered typical in reinforced concrete construction, however, because 3DPC structures are currently limited to 1-3 storeys in most applications while the cross section thickness is controlled by the need for stability during printing and space for insulation rather than structural demands, this leads to comparatively small axial load and larger wall cross-sectional areas, leading to lower anticipated axial load ratios. The computed axial load was based on the load in a first storey shear wall of a three storey structures.

After application of the gravity loading, it was maintained using load control and the in-plane cyclic loading protocol was applied. The protocol involved the application of two repeated cycles at increasing drift levels up to failure. Target drift levels were calculated based on the distance from the top of the wall foundation to the centreline of the cap beam (2815 mm in Figure 6). Panels were loaded in displacement control at an initial rate of 0.5 mm/min up to yielding of the reinforcement Subsequently, the loading rate was increased to 1.0 mm/min up to the end of the test. The test was stopped at the onset of brittle failure or a lateral deflection of ~100 mm (corresponds to drift of 4 %), whichever occurred first.

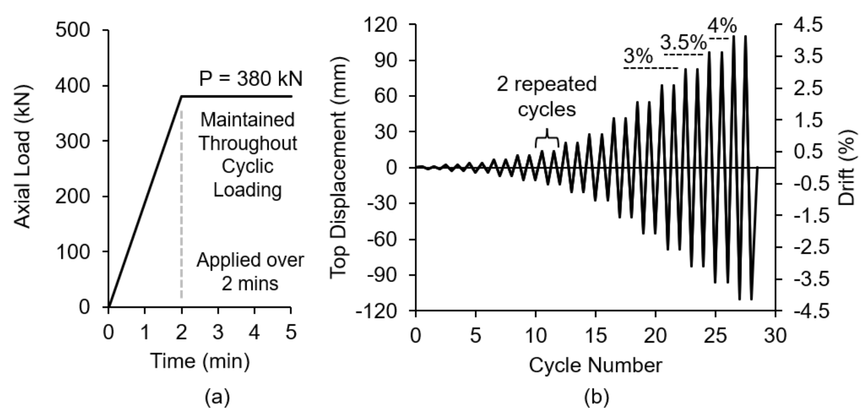

Figure 9. Loading protocol: (a) gravity loading, (b) reversed cyclic loading protocol.

EXPERIMENTAL RESULTS AND DISCUSSION

Table 2 summarizes the key structural response parameters for the 3DCP shear walls panels tested in this study, including the initial stiffness (k_i), cracking load (P_{cr}), deflection at yield (Δ_y), maximum load (P_{max}), deflection and drift at ultimate (Δ_{ult}). The initial stiffness was determined by fitting a line through the load versus deflection response of the specimens between 10% of the maximum load and the cracking load.

Table 2. Summary of test results

Wall Name	$P_{gravtiy}$ (kN)	k_i (kN/mm)	V_{cr} (kN)	Δ_y (mm)	V_{max} (kN)	M_{max} (kN-m)	Δ_{ult} (mm)	Δ_{ult} (%)	Failure Mode
S2	-	23.9	37.0	10.6	66.9	184	15.4	0.56	Lap Splice
			-50.0	-	27.4	75.4	-56.0	2.0	Pullout
S3	390	69.0	119	-	103	282	54.9	2.0	Yielding/Pullout
			-147	-16.1	155	-427	-40.8	1.5	Pullout
S4	390	80.6	159	14.0	164	453	82.0	3.0	Yeilding/Rupture
			-192	-16.2	-140	-394	-82.0	-3.0	Yielding/Rupture

Note:

Load-Deflection Behaviour and Failure Modes

Figure 5 shows the load-deflection hysteretic behaviour for wall panels S1 and S2 tested in this study. The results show that both walls exhibit a complex hysteretic behaviour, depending on the observed failure mode and level of axial load. In wall S2, which was tested without axial load, the wall exhibited an initial stiffness of 23.9 kN/mm, up to the average cracking load of approximately 43.5 kN on average. In the negative displacement direction, the wall experienced a premature pullout of the reinforcing bar embedded in the foundation block. Figure 11 shows the wall during testing, which showed significant uplift concentrated at the wall base. In the positive loading direction, the wall did not experience premature failure and the longitudinal reinforcement yielded at a moment of approximately 150 kN-m, which corresponds to the expected yield moment based on the geometry shown in Figure 1 and the properties of the bar. After yielding in the positive direction, the lap splice failed at a drift of approximately 0.56 %, which resulted in a sudden drop in the load carrying capacity. For conventional construction, in which significant ductility would not be required from a shear wall, this behaviour is acceptable and the wall achieves a maximum ductility of approximately 1.5. Finally, one of the novelties of this work was the use of closed stirrups at the layer-to-layer interfaces, which included both steel or GFRP stirrups in this work. Results of the study demonstrated that premature diagonal tension shear failure was prevented in both cases and diagonal cracking was limited, suggesting that these stirrups were an effective reinforcement configuration for 3DCP shear walls. No challenges associated with layer-to-layer bond at the levels of the stirrups were observed.

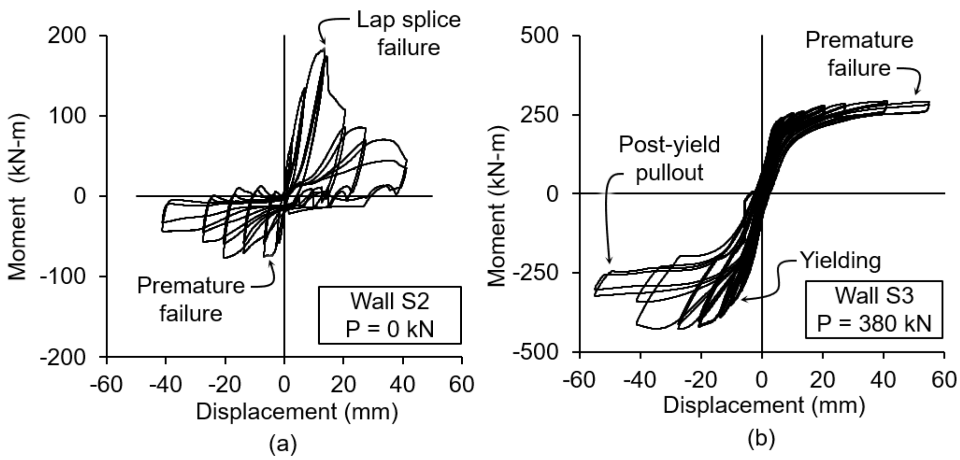

Figure 10. Moment versus displacement hysteretic behaviour of walls: (a) S2, (b) S3.

One of the observed challenges associated with the performance of the S2 wall was premature pullout of the longitudinal reinforcement from the foundation block, as highlighted in Figure 11. After removing the wall from the foundation block, it was discovered that the required embedment length (approximately 200 mm) was less than the target design embedment length of 300 mm. This discrepancy likely led to premature failure of the shear wall in that loading direction. This highlights the challenges associated with placement of reinforcement in 3DCP and the need to ensure construction tolerances are maintained as much as possible during what it a busy printing process. Future work could consider the use of mechanical coupling devices for the longitudinal reinforcement at the wall base, which would eliminate the need to rely on a post-installed adhesive and potentially be installed prior to the start of printing.

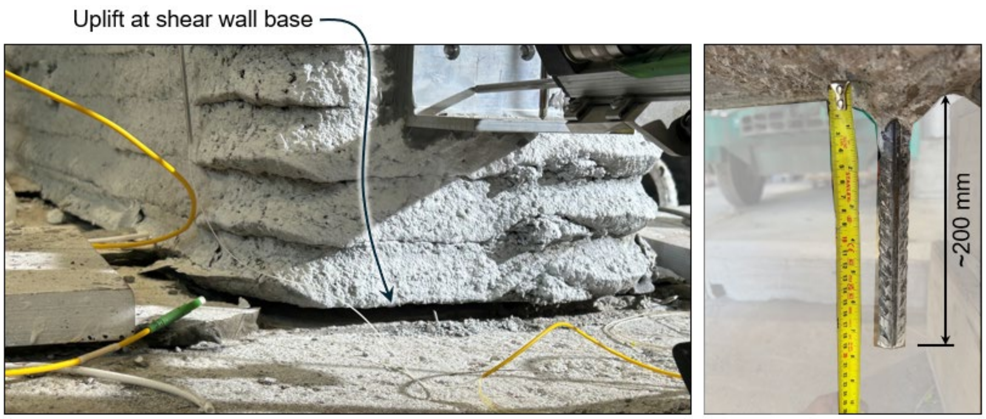

Figure 11. Observed failure mode in wall S2.

Figure 10(b) shows the moment versus drift hysteretic behaviour for wall S3, which included the application of axial load. The results show that the addition of axial load results in a significant increase in the initial stiffness of the wall, which was 69 kN/mm, which is approximately 35 % higher than the nominally identical wall without axial load. In the positive loading direction, wall S3 once again experience premature pullout failure, similar to wall S2 because of inadequate embedment of the longitudinal reinforcement. However, in the negative direction the wall exhibited the expected behaviour and the longitudinal reinforcing bar yielded in tension. The wall achieved a maximum moment resistance of 427 kN-m, which once again matches the design target, indicating suitable performance. At a lateral drift of approximately 1.25 %, the bar pullout from the foundation block after yielding, as noted by the drop in the moment-resistance beyond 1.5 % drift. However, this occurred at a ductility of 2.5, which is above what would be required for conventional construction in Canada, indicating that the wall exhibited adequate seismic performance in that loading direction.

Figure 12 shows the moment versus lateral drift response of wall S4, which had gravity load applied during the test and included confined boundary elements at the wall ends. The results show that because of the smaller bar size (3-10M bars instead of 1-20M bar) and a similar bar embedment depth, the walls did not experience the premature pullout failure that was observed in other wall specimens. The initial stiffness of the wall was 80.6 kN/mm, which is similar to Wall S3 because it had a similar area of longitudinal reinforcement. Small differences in the initial stiffness between these specimens is attributed to specific placement of the longitudinal bars in the cross-section, as bars in Wall S4 would have been placed closer to the wall ends, increasing the flexural lever arm. The longitudinal reinforcement yielded at a lateral drift of approximately 0.5 %, and the wall achieved an average maximum moment-resistance of 425 kN-m in each direction. No extensive diagonal cracking was observed in these tests, indicating that the horizontal shear reinforcement was once again effective at preventing premature diagonal tension shear failure.

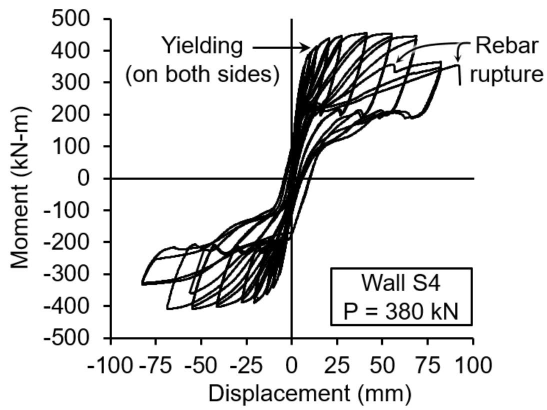

Figure 12. Moment versus displacement hysteretic behaviour of wall S4.

Post-yield response of the wall was characterized by uplift at the wall base and rupture of the longitudinal reinforcing bars in tension. Figure 13 show the deformed shape of the shear wall at the maximum drift of approximately 3.5% as well as photos of the damage experienced by the shear wall during the test. The results show that after yielding, extensive cracking and crushing at the toes of the wall was observed, as shown in Figure 13(b). This type of behaviour is expected in conventional reinforced concrete construction, and so, it is encouraging to see that type of behaviour in 3DCP walls. In addition to concrete crushing, rupture of the longitudinal reinforcement initiated at a lateral drift between 0.5 and 1% drift, starting first with the reinforcing bars located closest to the ends of the wall and progressively moving towards the centre of the wall. This behaviour is expected and is not detrimental to seismic performance because yielding occurred prior to rebar fracture. Ultimately, the wall achieved a displacement ductility above 5, which meets the requirements for a ductile shear wall according to Canadian design standards, indicating that 3DCP walls can achieve highly ductile seismic performance if they are adequately detailed. Furthermore, because of the unique deformation mechanisms in 3DCP walls, in which the comparatively low vertical reinforcement ratio relative to a conventional reinforced concrete wall leads to significant deformations at the wall base, resulting in 'rocking' behaviour under lateral loading. Because of the presence of gravity loading, this rocking behaviour results in a self-centering type hysteresis loop, in which the wall returns to its original position following a load cycle. This type of behaviour is advantageous from a seismic performance perspective because it reduces residual drifts following an earthquake.

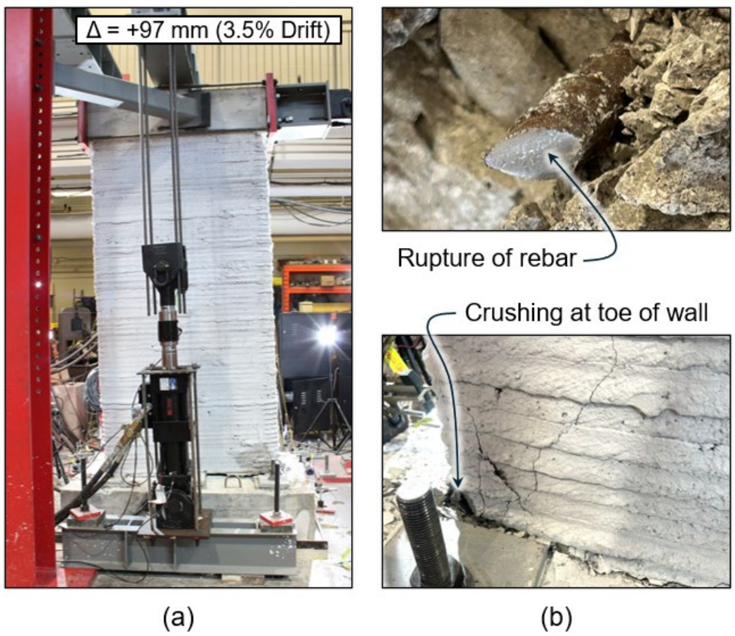

Figure 13. Observed failure modes in wall S4: (a) deformed shape at the ultimate drift, (b) typical rupture of longitudinal reinforcement, (c) observed crushing at the shear wall toes.

Analysis of Compression Strains from Digital Image Correlation

In addition to conventional discrete sensors to measure the wall performance, this study also examined the potential use of digital image correlation to measure surface strains and crack fields during a test. Figure 14 shows a sample result from the test on Wall S2. The results show that DIC was able to accurately localize the crack locations, even in a 3DCP shear wall with a very large region of interest. The cracks are shown to form at distinct locations along the wall height, including at the top of the lap splice of the vertical reinforcement, shown in Figure 1. This was expected as this location has the lowest reinforcement area relative to the applied moment over the height of the wall. Furthermore, the results from DIC showed that cracks had a tendency to form at the interface between 3DCP layers, rather than through the middle of a layer. This is partially attributed to the fact that there was no axial loading applied to this particular wall, and similar crack distributions in the other walls tested with gravity loading did not exhibit this tendency. These results show that the presence of axial load has a positive effect on the formation of cracking between layers.

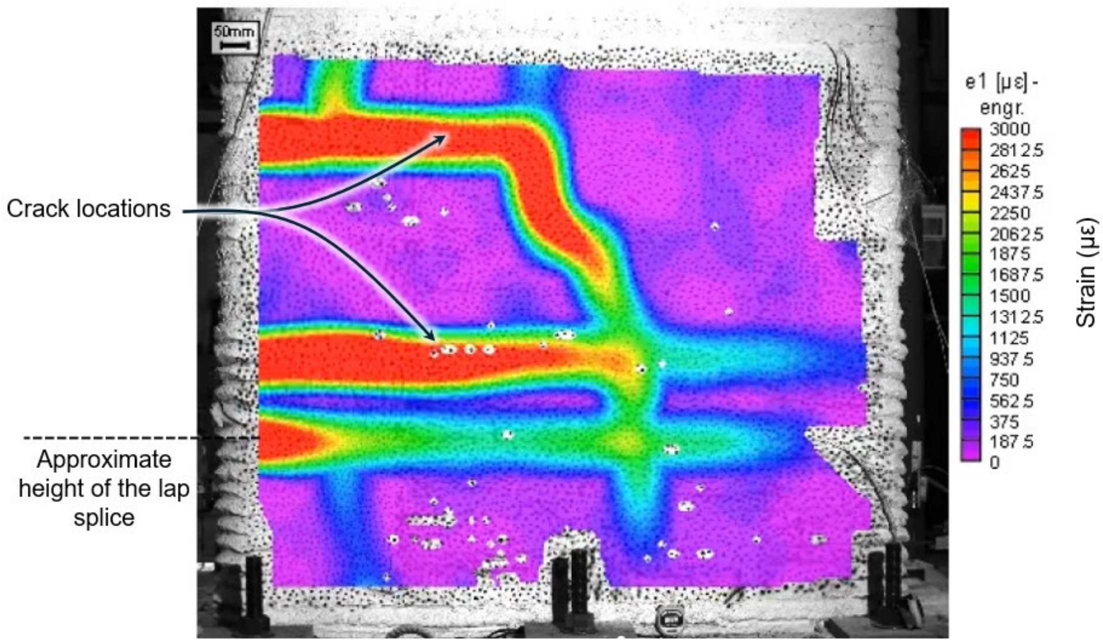

Figure 14. Typical strain and crack distribution in wall S2 (without gravity load).

CONCLUSIONS

This paper presents the results of an experimental study on the structural behaviour of 3DCP shear walls tested under axial and in-plane reversed cyclic loading. The influence of shear wall aspect ratio, boundary element reinforcement details, and axial load were investigated. Overall, the results of the study demonstrate that 3DCP shear walls can achieve the adequate seismic performance that is comparable to conventional reinforced concrete shear walls, if careful attention is paid to the reinforcement detailing and construction specifications. The specific conclusions of this study include:

1. The construction of a single-storey shear wall with longitudinal reinforcement can be achieved in practice, but requires careful consideration of construction sequencing and reinforcement detailing prior to construction.
2. Yielding of longitudinal reinforcement can be achieved without boundary element confinement, meeting the ductility requirements for conventional construction (ductility of 1.5 in this study).
3. 3DPC shear walls exhibit unique deformation mechanisms in their response under in-plane loading because of the strength of the base connection relative to the concrete wall panel, something that is more typical of precast concrete construction. This loads to more rocking in the shear wall response leading to self-centering hysteretic behaviour.
4. The use of horizontal stirrups of either steel or GFRP was found to be very effective at increasing the shear capacity of the 3DCP walls tested in this study. No issues associated with layer-to-layer bonding were observed during the experiments.
5. The use of confined boundary elements in 3DCP shear walls is very effective at improving ductility and energy dissipation capacity. The wall with confined boundary elements in this study achieved a displacement ductility of over 5, indicating that it could meet ductile shear wall performance according to Canadian standards.
6. Special attention needs to be paid during the construction of 3DCP walls to ensure that dimensions and tolerances are achieved. Because of the rapid nature of the construction technology, this means that crews need to be prepare for efficient and accurate construction. In this study, premature pullout failure was encountered because of inadequate embedment length during construction. This could be avoided in future work through the use of mechanical coupling devices, which could also potentially improve the speed of construction.

DATA AVAILABILITY STATEMENT

Some or all data, models, or code that support the findings of this study are available from the corresponding author upon reasonable request.

ACKNOWLEDGEMENTS

The authors gratefully acknowledge the financial support of the Federal Government of Canada (grant number RKI-1434). The material donation and technical assistance from Arektek (formerly Printerra) and MST Bar are also gratefully acknowledged. Technical assistance in the laboratory from Justin Bennett and Hal Stephens are also acknowledged.

NOMENCLATURE

The following symbols are used throughout this paper:

A_r	Area of longitudinal reinforcement (mm^2)
A_b	Area of reinforcing bar (mm^2)
f'_c	Concrete compressive strength (MPa)
f_r	Stress in the reinforcing bar (MPa)
f_y	Yield stress (MPa)
h_w	Wall height (mm)
k_i	Initial stiffness (kN/mm)
l_w	Wall length (mm)
M_r	Moment resistance (kNm)
P_{cr}	Cracking load (kN)
P_{max}	Maximum load (kN)
t_w	Overall wall thickness (mm)
Δ_y	Yield displacement (mm)
Δ_{ult}	Ultimate displacement (mm)
ρ	Reinforcement ratio (%)

REFERENCES

[1] Brozovsky, J., Labonnote, N., & Vigren, O. (2024). Digital technologies in architecture, engineering, and construction. Automation in Construction, 158, 105212.

[2] El-Sayegh, S., Romdhane, L., & Manjikian, S. (2020). A critical review of 3D printing in construction: benefits, challenges, and risks. Archives of civil and mechanical engineering, 20(2), 34.

[3] Mohamed, R. A., & Mohamed, A. F. A. (2025). Exploring the environmental benefits of 3D printing technology in concrete construction; a review. Progress in Additive Manufacturing, 10(1), 279-289.

[4] Zhang, J., Wang, J., Dong, S., Yu, X., & Han, B. (2019). A review of the current progress and application of 3D printed concrete. Composites Part A: Applied Science and Manufacturing, 125.

[5] Heidarnezhad, F., and Zhang, Q. (2022). Shotcrete based 3D concrete printing: State of art, challenges, and opportunities. Construction and Building Materials, 323, 126545.

[6] Cai, J., Wang, J., Zhang, Q., Du, C., Meloni, M., and Feng, J. (2024). State-of-the-art of mechanical properties of 3D printed concrete. Case Studies in Construction Materials, 21.

[7] Han, X., Yan, J., Liu, M., Huo, L., & Li, J. (2022). Experimental study on large-scale 3D printed concrete walls under axial compression. Automation in Construction, 133, 103993.

[8] Silveira, M. V., Wagner, J. S., Khanverdi, M., & Das, S. (2024). Structural performance of large-scale 3D-printed walls subjected to axial compression load. Canadian Journal of Civil Engineering, 51(8), 919-933.

[9] Khanverdi, M., & Das, S. (2025). Performance of full-scale 3D-printed concrete walls: Effects of vertical reinforcements and window opening. Engineering Structures, 337, 120510.

[10] Wang, J., Zhang, P., Feng, J., & Cai, J. (2024). Experimental study and design approach on 3D printed concrete walls under eccentric axial compression. Case Studies in Construction Materials, 20, e02892.

[11] Delavar, M. A., Chen, H., & Sideris, P. (2024). Analysis and design of 3D printed reinforced concrete walls under in-plane quasi-static loading. Engineering Structures, 303, 117535.

[12] Liu, C., Liang, Z., Liu, H., Wu, Y., Zhang, Y., & Bai, G. (2025). Seismic performance of 3D printed reinforced concrete walls: Experimental study and numerical simulation. Engineering Structures, 333, 120176.

[13] Aghajani Delavar, M., Sharma, S., Chen, H., Sideris, P., & Kreiger, E. (2026). Experimental Investigation on Full-Scale Shear-Critical 3D Printed Concrete Walls Subjected to In-Plane Cyclic Loading. Journal of Structural Engineering, 152(4), 04026019.

[14] Sritharan, S., Beyer, K., Henry, R. S., Chai, Y. H., Kowalsky, M., & Bull, D. (2014). Understanding poor seismic performance of concrete walls and design implications. Earthquake Spectra, 30(1), 307-334.

[15] Bruneau, M. (1994). State-of-the-art report on seismic performance of unreinforced masonry buildings. Journal of structural engineering, 120(1), 230-251.

[16] Ferreira, T. M., Costa, A. A., & Costa, A. (2015). Analysis of the out-of-plane seismic behavior of unreinforced masonry: A literature review. International Journal of Architectural Heritage, 9(8), 949-972.

[17] Wu, Z., Memari, A. M., and Duarte, J. P. (2022). State of the art review of reinforcement strategies and technologies for 3D printing of concrete. Energies, 15(1), 360.

[18] Kloft, H., Empelmann, M., Hack, N., Herrmann, E., & Lowke, D. (2020). Reinforcement strategies for 3D-concrete-printing. Civil Engineering Design, 2(4), 131-139.

[19] Asprone, D., Auricchio, F., Menna, C., & Mercuri, V. (2018). 3D printing of reinforced concrete elements: Technology and design approach. Construction and building materials, 165, 218-231.

[20] Buswell, R. A., De Silva, W. L., Jones, S. Z., & Dirrenberger, J. (2018). 3D printing using concrete extrusion: A roadmap for research. Cement and concrete research, 112, 37-49.

[21] Classen, M., Ungermann, J., & Sharma, R. (2020). Additive manufacturing of reinforced concrete—development of a 3D printing technology for cementitious composites with metallic reinforcement. Applied sciences, 10(11), 3791.

[22] Scott, C. (2016). Chinese Construction Company 3D Prints an Entire Two-Story House On-Site in 45 Days—3DPrint.com: The Voice of 3D Printing/Additive Manufacturing. (17 June 2016). Available online: https://3dprint.com/138664/huashang-tengda-3d-printhouse/ (accessed on March 3 2026).

[23] Hack, N., Lauer, W. V., Gramazio, F., & Kohler, M. (2014). Mesh-mould: Differentiation for enhanced performance. In Rethinking Comprehensive Design: Speculative Counterculture, Proceedings of the 19th International Conference on Computer-Aided Architectural Design Research in Asia (CAADRIA'14) (pp. 139-148). CAADRIA.

[24] Mechtcherine, V., Grafe, J., Nerella, V. N., Spaniol, E., Hertel, M., & Füssel, U. (2018). 3D-printed steel reinforcement for digital concrete construction–Manufacture, mechanical properties and bond behaviour. Construction and Building Materials, 179, 125-137.

[25] Kreiger, E. L., Kreiger, M. A., & Case, M. P. (2019). Development of the construction processes for reinforced additively constructed concrete. Additive Manufacturing, 28, 39-49.

[26] Sylaj, V., Fam, A., Hachborn H., and Burak, R. (2020). Flexural response of double-wythe insulated ultra-high-performance concrete panels with low to moderate composite action, PCI Journal, 65(1):24-40.

[27] Zhang, S. S., Yu, T., & Chen, G. M. (2017). Reinforced concrete beams strengthened in flexure with near-surface mounted (NSM) CFRP strips: Current status and research needs. Composites Part B: Engineering, 131, 30-42.

[28] Inkscape Project (2025). Inkscape. Retrieved from https://inkscape.org

[29] Wagner, J. S., Silveira, M. V., Vanderlei, R. D., & Das, S. (2024). Comparative analysis of mold-cast and 3D-printed cement-based components: implications for standardization in additive construction. Canadian Journal of Civil Engineering, 52(4), 388-404.

[30] ASTM International (2023). ASTM C39/C39M-23: Standard Test Method for Compressive Strength of Cylindrical Concrete Specimens. ASTM International, West Conshohocken, PA.

[31] ASTM International (2022). ASTM C78/C78M-22: Standard Test Method for Flexural Strength of Concrete (Using Simple Beam with Third-Point Loading). ASTM International.

[32] Sika (2023). Sika MonoTop-623 F: Product data sheet. Sika Canada Inc. Accessed from: https://can.sika.com/dam/dms/ca01/g/sika-monotop-623f.pdf

[33] Sika (2025). Sikadur-30: Product data sheet (Version 04.01). Accessed from: https://can.sika.com/dam/dms/ca01/4/sikadur-30.pdf

[34] Pultrall Inc. (2025). V-ROD Grade I Glass Fiber Reinforced Polymer (GFRP) rebar: Technical data sheet [Technical datasheet]. Accessed from: https://fiberglassrebar.com

[35] MST Rebar Inc. (2024). MST-BAR: Structural and Flat Work GFRP rebar technical data. MST Rebar Inc. Accessed from: https://mstbar.com/products/technical-data

[36] ASTM International (2024). ASTM E8/E8M-24: Standard Test Methods for Tension Testing of Metallic Materials. ASTM International. Accessed from: https://www.astm.org/Standards/E8_E8M.htm

[37] Correlated Solutions (2026). Non-contact, full-field strain, and deformation measurement system. Available from: https://www.correlatedsolutions.com/vic-3d. [Accessed March 4, 2026]

[38] CSA A23.3:24, Design of concrete structures, CSA Group, 2024.

[39] ACI 318-25, Building Code Requirements for Structural Concrete (ACI 318-25) and Commentary, American Concrete Institute, 2025.

[40] CSA S806:22, Design and construction of building structures with fibre-reinforced polymers, CSA Group, 2022.

[41] Carmo, R. N. F., Valença, J., Silva, D., & Dias-Da-Costa, D. (2015). Assessing steel strains on reinforced concrete members from surface cracking patterns. Construction and Building Materials, 98, 265-275.

[42] Brault, A., & Hoult, N. A. (2019). Distributed Reinforcement Strains: Measurement and Application. ACI Structural Journal, 116(4).